INTERNATIONAL JOURNAL OF HYDROGEN ENERGY 39 (2014) 8410–8420

Available online at www.sciencedirect.com

ScienceDirect

journal homepage: www.elsevier.com/locate/he

Thermal modeling and temperature control of a PEM fuel cell system for forklift applications

Vincenzo Liso [a,*], Mads Pagh Nielsen [a], Søren Knudsen Kær [a], Henrik H. Mortensen [b]

[a] Aalborg University, Department of Energy Technology, Denmark
[b] H2logic A/S, Denmark

ARTICLE INFO

Article history:
Received 19 February 2014
Accepted 22 March 2014
Available online 24 April 2014

Keywords:
Dynamic simulation
System modeling and control
PEMFC

ABSTRACT

Temperature changes in PEM fuel cell stacks are considerably higher during load variations and have a negative impact as they generate thermal stresses and stack degradation. Cell hydration is also of vital importance in fuel cells and it is strongly dependent on operating temperature. A combination of high temperature and reduced humidity increases the degradation rate. Stack thermal management and control are, thus, crucial issues in PEM fuel cell systems especially in automotive applications such as forklifts.

In this paper we present a control-oriented dynamic model of a liquid-cooled PEM fuel cell system for studying temperature variations over fast load changes. A temperature dependent cell polarization and hydration model integrated with the compressor, humidifier and cooling system are simulated in dynamic condition. A feedback PID control was implemented for stack cooling.

The stack energy balance was reduced to a first order differential equation using a lumped approach. The first-order Linear Time-Invariant system was used to obtain the transfer function which was determined based on experimental data at different stack loads. The developed model approach can assist designers in choosing the required coolant mass flow rate and radiator size to minimize the stack temperature gradients.

Introduction

An important requirement for fuel cell systems in automotive applications is to meet fast changing loads still providing proper stack cooling and hydration. In this regard, knowledge of the stack in terms of transient behavior is of critical importance. The dynamic behavior of a Proton Exchange Membrane Fuel Cells (PEMFC) system is strongly dependent on the reactant flows and the water and thermal management. Proper thermal and water management is in fact, also essential to achieve optimum performance from PEMFC stacks. Mathematical models play an important role in supporting the design and enhancing the understanding of the effect of parameters on the performance of the stack and fuel cell auxiliary systems.

In order to describe dynamics of stack temperature under various load conditions experimental data are to be combined with physical phenomena models with good level of approximation. First attempt to integrate a mechanistic model and

* Corresponding author.
E-mail address: vli@et.aau.dk (V. Liso).
http://dx.doi.org/10.1016/j.ijhydene.2014.03.175

Nomenclature

AR	Recycle ratio
E	Reversible cell voltage at standard conditions, V
F	Faraday's constant, C mol^{-1}
i	Fuel cell current density, A cm^{-2}
kA_{FC}	heat transfer coefficient for the fuel cell, W/K
$\dot{m}$	Mass flow rate, g/s
M	Molar mass, g/mol
N_{cell}	Cell number
$\dot{n}$	Molar flow rate, mol/s
p	partial pressure, bar
$\dot{Q}$	Heat flow rate, J/s
RPM	Rate per minute
T_{fc}	Fuel cell temperature, K
v	Fuel cell operating voltage, V
$\dot{V}$	Volume flow rate, l/s
V	Volume, m^3
y	Molar fraction

Greek symbol

λ_m	Membrane water activity, –
λ_{O_2}	Air stoichiometry or air excess ratio, –
τ	Time constant, s

Subscript

act	Activation
ca	cathode
conc	Concentration
fc	Fuel cell
in	Inlet
m	Membrane
ohm	Ohmic
out	Outlet

empirical data for predicting the stack temperature can be found in Ref. [1]. They developed a dynamic model for a Ballard Mark V PEM fuel cell stack, which calculate fuel cell voltage and stack temperature for a given set of gas feed and operating conditions. No control strategies were studied in this paper. Moreover, many publications addressed the water and thermal management of the fuel cell in order to describe the water, thermal and reactant utilization of fuel cell by means of two or three-dimensional models. Fuller and Newman [6] demonstrated the importance of thermal management while trying to maximize the performance of fuel cell stack used within a vehicle. Steady-state models are typically used for component sizing, static trade-off analysis or cumulative fuel consumption.

Pukrushpan [11] developed a control model of a fuel cell system however stack cooling was not investigated; instead fixed stack temperature was considered at every load. Vasu and Tangirala [13] expanded Pukrushpan model with a thermal dynamic model for predicting the stack temperature, temperatures of the exit reactant gases and coolant water outlet in a proton-exchange membrane fuel cell. Yu et al. [14] developed a water and thermal management model for a Ballard PEM fuel cell stack to investigate its performance. However the temperature control was not considered in these models. In Refs. [12,7], the authors conducted a parametric study in steady-state of the thermal performance and water management of low temperature Proton Exchange Membrane Fuel Cell Ballard stack Mark9 SSL™. The semi-empirical models for thermal management of a stack cannot be used directly for control studies due to the implicit forms of the expressions that are used to calculate the stack temperature.

A need exists for a technique for determining stack thermal performance that does not require extensive solution time. In addition, the model needs to be able to be integrated with a complete fuel cell stack thermal system. In this way, it is possible to determine stack temperature and other operating parameters to fully assess the performance of the thermal system especially in highly dynamic operating conditions such as automotive applications.

In the present work, control-orientated system-level dynamic models are developed for stack temperature dynamics by explicitly taking into account the heat loss to the surroundings in addition to convection, the sensible heat of coolant and reactants. These models are integrated with first-principle based models of an air flow compressor and the semi-empirical voltage–current model of Ref. [11]. The control analysis allows estimating the thermal behavior of the stack depending of the electrical load.

System description and methodological assumption

The Ballard FCvelocity 9SSL 21 kW stack used in this study consists of 110 cells. The active cell area is of 285.8 cm^2. Liquid cooling is provided by a mix of water and ethylene glycol. The stack weight approximately 17 kg. This stack is designed for motive applications. The fuel cell system considered in this study is simplified in Fig. 1.The stack is fueled by hydrogen stored in a pressure tank. Depleted anode gas is recycled by means of a compressor and an ejector. There is no external humidification apparatus for fuel as steam is fully provided by anode gas recirculation. Cathode air is first compressed and cooled down to 65 °C, after which it is humidified by a Nafion selectively permeable membrane. Water for the humidifier is provided by depleted cathode air. Finally, water from the air is collected in a water tank and excess air is expelled outside.

To avoid starvation and simultaneously match an arbitrary level of current demand, adding a rechargeable auxiliary power source which can respond quickly to the increase in

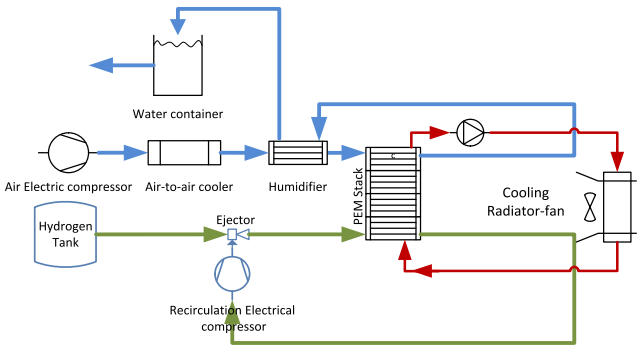

Fig. 1 – System pipe and instruments diagram.

current demand is necessary. Batteries or ultra-capacitors are power sources that respond relatively quickly to current demand. They can be used in parallel with a fuel cell to cover the high peaks in demand and can be recharged by the fuel cell itself, when the demand is lower. In order to reduce stack faults and degradation, fuel cell load ramp up and down is limited to 20 A/sec.

Different control schemes for each fuel cell stack parameter are adopted in this study. Feed-forward control algorithm is used to control cathode air and hydrogen mass flow rate based on the current drawn from the fuel cell. Coolant mass flow rate is also based on the current reference input. In these cases, look-up tables were implemented in Matlab/Simulink to relate parameters with current load. Coolant temperature is reduced by mean of a radiator-fan which is controlled by a PID controller.

The operating parameters that must be set in the program are air and fuel inlet stoichiometry, inlet pressure, pressure drop, relative humidity, and the operating temperature of the stack. All simulations are performed under the MATLAB/Simulink and Simscape environment. The differential equation solver ODE23s is employed as it resulted more computationally efficient than other solvers in presence of mild stiffness.

We assume an averaged stack temperature; reference stack temperature is set to 65 °C. We also assume that the inlet reactant flows in the cathode and anode can be humidified, heated and cooled in a consistent and rapid way. Although this assumption will not be always true, especially during fast transients loads. Faster changes of the external load were assumed handled by an additional battery.

Fuel cell model

In this section, a nonlinear dynamic model of the fuel cell is developed using electrochemical, thermodynamic and zero-dimensional fluid mechanics principles.

Electrochemical model

The fuel cell operating voltage v_{fc} [volts] is calculated as follow:

$$\begin{aligned} v_{fc} &= E - v_{act} - v_{ohm} - v_{conc} \\ &= E - a_1\left[v_o + v_a\left(1 - e^{-c_1 i}\right)\right] - a_2 i R_{ohm} - a_3\left[i\left(c_2\frac{i}{i_{max}}\right)^{c_3}\right] \end{aligned} \quad (1)$$

where the limiting current density $i_{max} = 2.2$ [A/cm^2] and calibrating parameter $a_{1,2,3}$ and $c_{1,2,3}$ are fixed as follow:

$$\begin{aligned} &a_1 = 0.9;\ \ a_2 = 20;\ \ a_3 = 0.9 \\ &c_1 = 10;\ \ c_2 = \left(7.16\times10^{-4}T_{fc} - 0.622\right)\left(\frac{p_{O_2}}{0.1173} + p_{sat}\right) \\ &\qquad + \left(-1.45\times10^{-3}T_{fc} + 1.68\right);\ \ c_3 = 2 \end{aligned} \quad (2)$$

Using thermodynamic values of the standard state entropy change, the open circuit voltage, E, can be written as a function of T_{fc} and hydrogen and oxygen partial pressure [1]:

$$\begin{aligned} E = 1.229 - 8.5\times10^{-4}\left(T_{fc} - 298.15\right) + 4.3085\times10^{-5}T_{fc}\left[\ln\left(p_{H_2}\right)\right. \\ \left. + 0.5\ln\left(p_{O_2}\right)\right] \end{aligned} \quad (3)$$

Reversible cell voltage at standard conditions, E, was calculated via the lower heating value (1.254 V − LHV) if the generated water is in vapor form.

Single cells are stacked up in series to form a fuel cell stack; the total voltage of the stack is obtained by multiplying the total number of cells by the single cell voltage. Voltage empirical parameter v_o and v_a [volts] are provided below:

$$\begin{aligned} v_o &= 0.279 - 8.5\times10^{-4}\left(T_{fc} - 298.15\right) \\ &\quad + 4.308\times10^{-5}\left[\ln\frac{p_{ca} - p_{sat}}{1.01325} + \frac{1}{2}\ln\frac{0.1173\left(p_{ca} - p_{sat}\right)}{1.01325}\right] \\ v_a &= \left(-1.618\times10^{-5}T_{fc} + 1.618\times10^{-2}\right)\left(\frac{p_{O2}}{0.1173} + p_{sat}\right)^2 + \left(1.8\right. \\ &\quad \left.\times10^{-4}T_{fc} - 0.166\right)\left(\frac{p_{O2}}{0.1173} + p_{sat}\right) + \left(-5.8\times10^{-4}T_{fc}\right. \\ &\quad \left. + 0.5736\right) \end{aligned} \quad (4)$$

The calculation of v_o and v_a requires the knowledge of cathode pressure (representing total pressure), p_{ca} [bar], oxygen partial pressure, p_{O_2} [bar], and fuel cell temperature, T_{fc} [K]. R_{ohm} is the internal electrical resistance which has units of Ω cm^2. The resistance depends strongly on the membrane humidity and the cell temperature. Ohmic resistance is a function of the membrane conductivity, σ_m [(Ω cm)$^{-1}$], in the form:

$$\begin{aligned} &R_{ohm} = \frac{t_m}{\sigma_m} \quad with: \\ &t_m = 0.0125 \\ &\sigma_m = b_1\exp\left(b_2\left(\frac{1}{303} - \frac{1}{T_{fc}}\right)\right) \\ &b_1 = 0.005139\ \ \lambda_m - 0.00326;\ \ b_2 = 350 \end{aligned} \quad (5)$$

where t_m [cm] is the thickness of the membrane and the membrane conductivity; σ_m, is a function of membrane water content; λ_m is the membrane water activity presented in the next section, and T_{fc} is fuel cell temperature [K]. The value of λ_m varies between 0 and 14. A full list of parameters used throughout this paper is provided in Table 1.

Table 1 – Fuel cell parameters.

Parameter	Description	Value	Ref
n_{fc}	Number of cells [–]	110	[2]
A_{fc}	Fuel cell active area [cm^2]	285.8	[2]
V_a	Anode volume [m^3]	0.014	[2]
V_c	Cathode volume [m^3]	0.00078	[2]
V_{stack}	Stack Volume [m^3]	0.014	[2]
F	Faraday constant [C mol^{-1}]	96,485	
ΔH	Hydrogen enthalpy of combustion [kJ mol^{-1}]	285.5	
C_t	Thermal capacitance [kJ C^{-1}]	17.9	[1]
$C_{p,coolant}$	Heat capacity of water [kJ kg^{-1} K^{-1}]	4.184	
t_m	Membrane thickness [cm]	5.1×10^{-3}	[10]
$M_{m,dry}$	Membrane dry eqv weight [kg mol^{-1}]	1.1	[8]
$\rho_{m,dry}$	Membrane dry density [kg cm^{-3}]	0.002	[9]
R	Universal gas constant [J mol^{-1} K^{-1}]	8.314	

Table 2 – Fuel cell stack operating conditions depending in current.

Parameters depending on stack current							
Stack Current [A]	15	30	60	120	180	240	300
Cell Voltage [V]	0.8570.	8250	0.7880	0.7420	0.7150	0.6830	0.643
Stack Power [W]	1414	2722	5200	9794	14,157	18,031	21,219
Fuel Inlet Stoichiometry Min.	6.3	3.4	2.2	1.9	1.6	1.6	1.6
Oxidant Inlet Stoichiometry Min.	5.1	2.4	1.8	1.8	1.8	1.8	1.8
Nominal Inlet Temperature Relative to Coolant [°C]	1	1	1	1	1	1	1
Coolant Inlet Temperature Max. [°C]	60	60	60	60	60	60	60
Coolant Outlet Temperature Max. [°C]	61	63	66	67	68	68	70

In Table 2 fuel cell stack operating conditions depending on reference current are presented. These experimental data are provided according to Ref. [2].

Membrane hydration model

Water content is fuel cell membrane is a crucial operational factor. Too low water content will compromise the conductivity of the membrane, whereas too much water will flood the cathode and block the flow through the porous layer. As a result, water management is dealt with by humidifying the gas flows entering the stack and forcing the cathode gas flow to pass all the cathode sides in parallel, to mechanically remove any liquid water.

The two phenomena which dominate the water transport are:

- Water transport due to electro-osmotic drag by protons from the anode to the cathode

$$\dot{n}_{H_2O,m,osmotic} = n_d \frac{i}{F} \tag{6}$$

n_d, which is defined as the number of water molecules carried by each proton [mol s^{-1} cm^{-2}]i, is the fuel cell current density [A cm^{-2}]F, is the Faraday constant [C mol^{-1}]

- Back diffusion of water caused by concentration gradients from the cathode to the anode

$$\dot{n}_{H_2O,m,backdiff} = D_w \times \frac{dc_{H_2O}}{dy} \tag{7}$$

D_w is the diffusion coefficient of water in the membrane [cm^2 s^{-1}]c_{H_2O} is the water concentration in the membrane [mol cm^{-3}]y is the perpendicular distance into the membrane [cm]

Exposing the fuel cell to low or zero current conditions has been shown to lead to higher degradation rates and increase in hydrogen cross-over in comparison to operation at a constant current [4]. For this reason low current density are avoided in the fuel cell system operation and power is provided by an additional battery pack.

Combining water osmotic drag and back diffusion equations, the following equation for the resulting water transport is drawn:

$$\dot{n}_{H_2O,m} = \dot{n}_{H_2O,m,osmosis} - \dot{n}_{H_2O,m,backdiff} \tag{8}$$

The net water flux $\dot{n}_{H_2O,m}$ will be positive if the transport is in the direction from the anode to the cathode. The water concentrations at the membrane surfaces are found by:

$$c_{H_2O,i} = \frac{\rho_{m,dry}}{M_{m,dry}} \lambda_i \tag{9}$$

where i represents either anode, cathode or membrane, $r_{m,dry}$ is the density of the dry membrane [kg/cm^3] and $M_{m,dry}$ is the equivalent weight of the dry membrane [g/mol].

The water content in the membrane was measured by Zawodzinski et al. [15] and can be found from the following equations depending on water activity:

$$\lambda_i = \begin{cases} 0.043 + 17.81a_i - 39.85a_i^2 + 36.0a_i^3 & ,0 \le a_i \le 1 \\ 14 + 1.4(a_i - 1) & ,1 < a_i \le 3 \end{cases} \tag{10}$$

$$n_d = 0.0029\lambda_m^2 + 0.05\lambda_m - 3.4 \times 10^{-19} \tag{11}$$

The water activity (ratio of the partial pressure of vapor and the saturation pressure) of the membrane is found as the mean value between the anode and cathode water activity.

The water diffusion coefficient is calculated from:

$$D_w = D_\lambda \cdot \exp\left(2416 \cdot \left(\frac{1}{303} - \frac{1}{T_{fuel\ cell}}\right)\right) \tag{12}$$

where D_λ depends on the water content in the membrane. Dutta et al. [5] used the following relations:

$$D_\lambda = \begin{cases} 10^{-6} & ,\lambda_m < 2 \\ 10^{-6}(1 + 2(\lambda_m - 2)) & ,2 \le \lambda_m \le 3 \\ 10^{-6}(3 + 1.67(\lambda_m - 3)) & ,3 \le \lambda_m \le 4.5 \\ 1.25 \times 10^{-6} & ,\lambda_m \ge 4.5 \end{cases} \tag{13}$$

As air and hydrogen stack inlet streams are considered with good humidification, the water content λ_m will stay in the high end range (i.e.$\lambda_m \ge 4.5$).

Pressure driven gradients can be used to force water through the membrane but this is limited by the strength of the membrane. Usually manufacturers do not recommend a differential pressure more than 0.5–1 bar since higher pressures would lead to permanent damage of the membrane. Another issue is crossover of hydrogen, which would react with oxygen on the cathode side and lead to undesirable oxidation.

The membrane water content and the rate of mass flow across the membrane are functions of the stack current and relative humidity of the reactants in the anode and the cathode flow channels. By increasing current density, drag force term dominates on diffusion term in the governing Equation (13). This causes higher water content at low current densities both at anode and cathode. In order to avoid membrane flooding, both air and hydrogen stoichiometry are maintained particularly high at lower loads. In Fig. 2, fuel cell water content at different loads is plotted. Due to cell temperature variations during load changes, it takes some times to reach

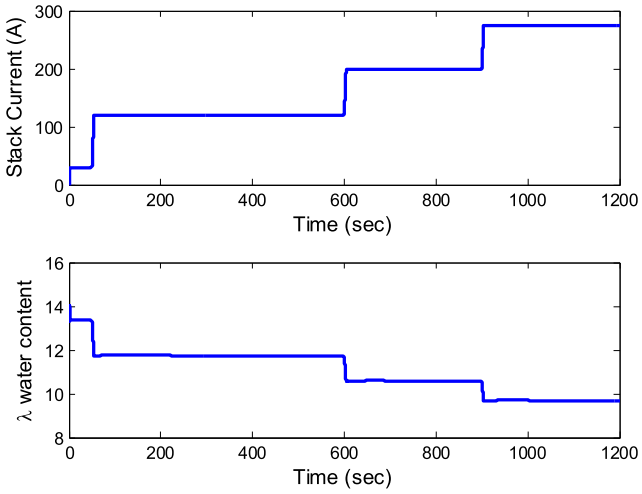

Fig. 2 – Effect of the electro-osmotic drag on the membrane water content at different stack currents.

stationary condition once load is changed. The reduction of average cell water content due to load changes is evident in Fig. 3. Air and hydrogen inlet flows streams are kept at good humidification (i.e. 95% RH); this ensures high λ values and relatively small range of variation in cell water content.

In Fig. 3 the calibration results of the model against the experimental data provided in Ref. [2] is provided. It is important to mention that in order to reduce fuel cell degradation, low and high current density values are usually avoided mainly due to high degradation in these operational ranges [4].

Anode and cathode flow models

Anode and cathode dynamic flow model are modeled in a lumped fashion. Chemical reaction and water transport between the anode and the cathode cause the variation of components. Therefore, every species is treated independently. Current, I; is considered as input and hydrogen and air mass flow rate is calculated as a function of reference stack current.

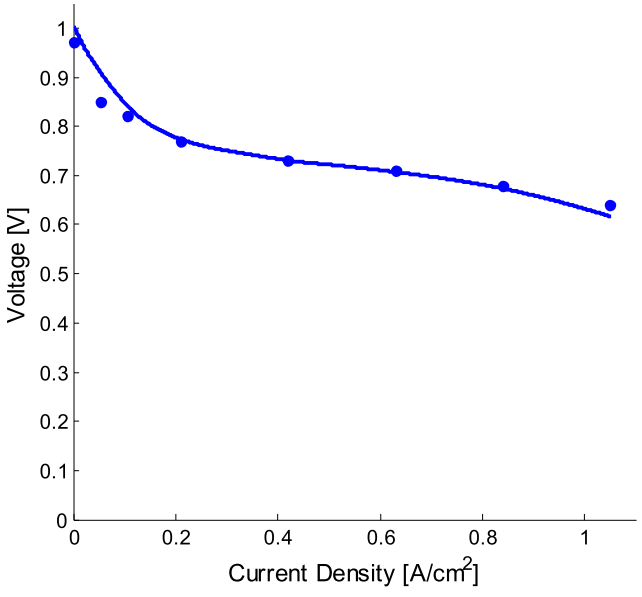

Fig. 3 – Fuel cell polarization curve calibration against experimental data from Ballard.

Anode flow model

The mass conservation of hydrogen in the anode can be described as:

$$\frac{d\dot{m}_{H_2,an}}{dt} = \dot{m}_{H_2,\tan k} + AR \times \dot{m}_{H_2,an,out} - \frac{I_{stack}N_{cell}}{2F} - \dot{m}_{H_2,an,out} \quad (14)$$

where I_{stack} is the stack current, N_{cell} the number of cells and F the Faraday constant, $\dot{m}_{H_2,\tan k}$ is the hydrogen mass flow rate from the pressure tank. AR represents the ratio between the recycled anode gas and the total anode outlet mass flow The anode inlet mass flow rate $\dot{m}_{H_2} = \dot{m}_{H_2,\tan k} + AR \times \dot{m}_{H_2,an,out}$ is imposed according to experimental data available in Ref. [2]:

$$\dot{m}_{H_2} = 0.7656 \times I \times \rho^{\ominus}_{H_2} \quad (15)$$

where $\rho^{\ominus}_{H_2} = 0.089$ g/L is the hydrogen density at standard conditions. The mass conservation of vapor in the anode is calculated as:

$$\frac{d\dot{m}_{vap,an}}{dt} = \dot{m}_{vap,an,in} + AR \times \dot{m}_{vap,an,out} - \dot{m}_{vap,membr} - \dot{m}_{vap,an,in} \quad (16)$$

$\dot{m}_{vap,membr}$ is calculated from Equation (8). $\dot{m}_{vap,an,in}$ is calculated considering 95% *RH*. The water in the anode is considered only in the gaseous phase. The anode mixture pressure can be expressed according to the ideal gas law:

$$p_{an} = R \cdot T \cdot V_{an}\left(\dot{m}_{H_2,an}/M_{H_2} + \dot{m}_{vap,an}/M_{H_2O}\right) \quad (17)$$

where V_{an} is the anode volume. In the cathode, oxygen reacts and water generates. Unlike to the anode, phase change of water in the cathode is considered in this paper.

Anode recirculation

There are not many descriptions of the recirculation loop for the hydrogen in the open literature [3]. In general, the inlet flow of the anode is obtained by mixing the flow coming from the recirculation and the flow of dry hydrogen coming from the tank inside the ejector.

The pressure inside the recirculation system has to be higher than the pressure at the inlet, in order to avoid counter flow inside the recirculation system. The anode inlet pressure has to be controlled considering cathode channel pressure in order to avoid different pressures of the two inlet streams.

Consequently, the inlet mass flow-rate in the anode channel can be calculated by the sum of the mass flow-rate of the recirculation stream and the hydrogen coming from the tank.

$$\dot{m}_{an,in} = \dot{m}_{tank,in} + \dot{m}_{recirc,H_2} \quad (18)$$

The temperature of this inlet stream is fixed as shown in table.

Cathode flow model

The amount of air necessary as well as the desired operating air pressures is sufficiently high to cause large electrical parasitic loads at the compressor motor. Because of this, when the fuel cell system is not operating at full power (a majority of the time), the air system output needs to be reduced as well. This now requires a variable flow and pressure air system that results in complex component designs and expensive controllers with a variable speed motor. Air mass flow rate input is calculated as a function of stack current I and oxygen excess ratio λ_{O_2}. The latter is imposed according to data presented in Table 2.

$$\dot{m}_{ca,in} = 1.2826 \times \rho_{Air}^{\ominus} \cdot I \cdot \lambda_{O_2} \tag{19}$$

$\rho_{Air}^{\ominus}$ is the air density at standard conditions. High oxygen excess ratio λ_{O_2} corresponds to more oxygen supplied to the cathode, which improves the power generated by the stack. However, if λ_{O_2} is too large, then net power decreases due to excessive power demanded by the air compressor. As a result, there exists an optimal value for λ_{O_2} that maximizes the net power by trading off stack power production and compressor motor power consumption.

The species variation in the cathode can be described by:

$$\frac{d\dot{m}_{O_2}}{dt} = \dot{m}_{ca,in} y_{O_2,in} - \frac{I_{stack} N_{cell}}{4F} - \dot{m}_{ca,out} y_{O_2,ca} \tag{20}$$

$$\frac{d\dot{m}_{N_2}}{dt} = \dot{m}_{ca,in} y_{N_2,in} - \dot{m}_{ca,out} y_{N_2,ca} \tag{21}$$

$$\frac{d\dot{m}_{vap,ca}}{dt} = \dot{m}_{ca,in} y_{vap,ca,in} + \frac{I_{stack} N_{cell}}{2F} M_{H_2O} + \dot{m}_{vap,membr} - \dot{m}_{ca,out} y_{vap,ca} \tag{22}$$

where $\dot{m}_{O_2}$, $\dot{m}_{N_2}$ and $\dot{m}_{vap,ca}$ are the mass flow rate of oxygen, nitrogen and vapor in the cathode, respectively. Here, the water generated and transported from the anode are both considered in the gaseous phase, and the mass of liquid water in the cathode, $\dot{m}_{liq,ca}$, is introduced to reflect the accumulation of liquid water in the cathode flow channel. The inlet species mass fractions y_{O_2} and y_{N_2}. $y_{vap,in}$ is decided by the thermodynamic condition of the mixture in the cathode humidifier considering a relative humidity $RH = 95\%$. According to the ideal gas law, the cathode mixture pressure should be:

$$p_{ca} V_{ca} = RT\left(\dot{m}_{O_2,ca}/M_{O_2} + \dot{m}_{N_2,ca}/M_{N_2} + \dot{m}_{vap,ca}/\dot{m}M_{H_2O}\right) \tag{23}$$

where V_{ca} here is the cathode volume.

Air compressor model

The pressure drop rapidly increases to very high levels in the cathode channel, with increasing costs and loss of efficiency of the fuel-cell system. The energetic cost of the air compressor is by far the largest one among ancillary units. However, operating all cells in parallel, with all cells connected to the same entering and exiting manifolds, may block some cells where flooding is occurring. As the gases will take the path of least resistance, these cells will remain flooded. Again, because of the usual electrical series connections, flooding of a single cell can reduce the whole stack's current as the flooded cell will work as an electrical resistance. Any approach to manage a membrane's water content based on feedback control suffers from the fundamental problem that the liquid water content in each cell is difficult to measure: both dry-out and flooding will result in a drop in voltage. For this reason a feed-forward control of the air mass flow rate based on the stack current reference was used.

This model is based on compressor specification sheet reported in Fig. 4:

$$RPM_{Comp} = \dot{V}_{Air} \times p_{drop} \tag{24}$$

$$P_{comp} = RPM_{Comp} \times p_{drop} \tag{25}$$

Pressure drops p_{drop} [bar] is experimentally measured and data are reported in Table 3 [2]. Compressor performance and pressure drop are shown in Fig. 5.

Humidifier model

As shown in Fig. 1, air is humidified after being compressed and cooled down. Humidification is achieved by a Nafion selectively permeable membrane tubing and liquid water to continuously humidify gas streams. Inlet cathode air is fixed with 95% relative humidity (*RH*).

On the anode side, hydrogen is warmed up and humidified by the recycled anode gas and water crossover from cathode to anode. It is assumed that *RH* of the mixture in the anode

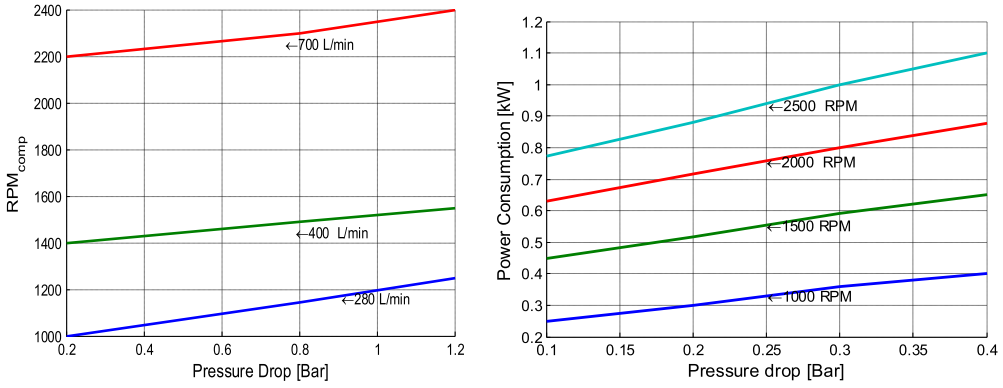

Fig. 4 – Compressor characteristics.

Table 3 – Cell anode–cathode pressure difference.

Fuel cell performance parameter							
Stack Current [A]	15	30	60	120	180	240	300
Pressure difference [kPa]	6	6	13	19	34	44	55

around 95%; this can be considered a rough estimation as RH varies with temperature, load etc.

For simplicity, the humidification of gases is considered to be perfect. A static model based on the mass conservation is used in the humidifiers. The *RH* is defined as:

$$RH = y_{H_2O} \times p_g \Big/ p_{sat}(T) \tag{26}$$

where y_{H_2O} is the molar fraction of water in the gas stream, p_g is the gas phase pressure and p_{sat} is the saturation pressure as function of temperature. Clearly, the higher the gas phase pressure is for a given molar composition, the higher is the *RH*, and accordingly the dew point temperature will increase with increasing pressure. The saturated pressure is related to temperature according the following equation [7]:

$$\log(p_{sat}) = \left(-2.1794 + 0.02953T - 9.1837 \times 10^{-5}T^2 + 1.4454 \times 10^{-7}T^3\right) \tag{27}$$

The temperature of the flow is assumed constant. The water injected is assumed to be in the form of vapor and the latent heat of vaporization is assumed to be taken into account in the air cooler. The amount of vapor injected in the air is calculated by comparing the vapor flow at the air cooler outlet and the required vapor flow for the desired humidity.

System thermal model

Generally, heat generation Q [Watts] in one cell can be calculated from:

$$Q = (E_{nernst} - V_{cell}) \times I \tag{28}$$

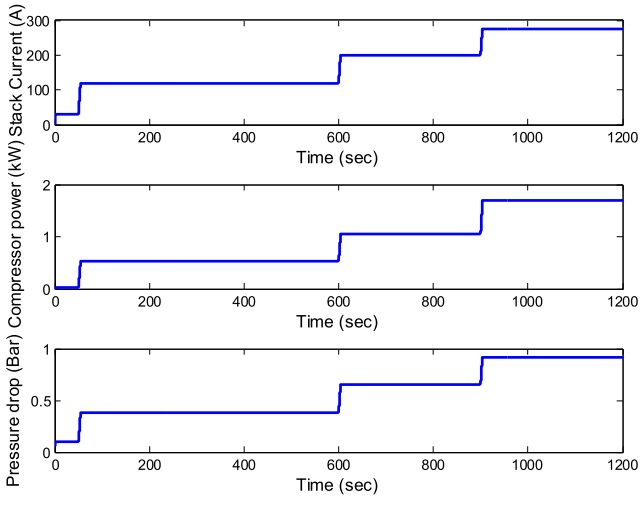

Fig. 5 – Air compressor power usage and cathode pressure drop at different stack load.

where the reversible cell voltage, E_{nernst}, should be calculated by the lower heating value (1.254 V) if the generated water is in vapor form. To maintain the operating temperature of the stack within the desired range part of this heat should be removed from the stack. The stack heat dissipation is achieved mainly by conduction and convection. Cooling medium may be air or liquid. Small stack can be cooled by air; this is not efficient in stacks larger than 10 kW as the one under study. In this case liquid cooling is usually adopted.

With reference to Fig. 6, the coolant is circulated through the stack by a pump. The heat is indirectly transferred from the hot coolant flow stream to the cold airflow stream by means of a radiator-fan.

The coolant mass flow rate is dictated by the fuel cell load by feed-forward control of the coolant pump. The heat in the coolant is dissipated by means of a radiator-fan. Fan speed is controlled by a PID controller using the fuel cell temperature as a reference, $T_{stack} = 65\ ^\circ C$.

The energy balance can be written as follows:

$$MC_{stack}\frac{dT_{stack}}{dt} = \dot{E}_{tot} - \dot{Q}_{sens} - E_{elec} - \dot{Q}_{coolant} - \dot{Q}_{Conv} \tag{29}$$

where MC_{stack} [kJ/K] is the thermal mass of the fuel cell stack and dT_{stack}/dt is the temperature change with respect to time. Other equation terms are specified below:

$$\begin{aligned}
\dot{E}_{tot} &= -\frac{nI}{2F}\Delta H \\
\dot{Q}_{sens} &= \dot{Q}_{in,sens} - \dot{Q}_{out,sens} \\
\dot{E}_{elec} &= V_{stack} I \\
\dot{Q}_{coolant} &= \dot{m}_{coolant} \times C_{p,coolant} \times \left(T_{coolant,out} - T_{coolant,in}\right) \\
\dot{Q}_{aircool} &= \dot{Q}_{coolant} = \dot{m}_{air} \times C_{p,air} \times \left(T_{air,out} - T_{air,in}\right) \\
\dot{Q}_{Conv} &= k_{Conv} \times A_{Stack} \times \left(T_{FC} - T_{Amb}\right)
\end{aligned} \tag{30}$$

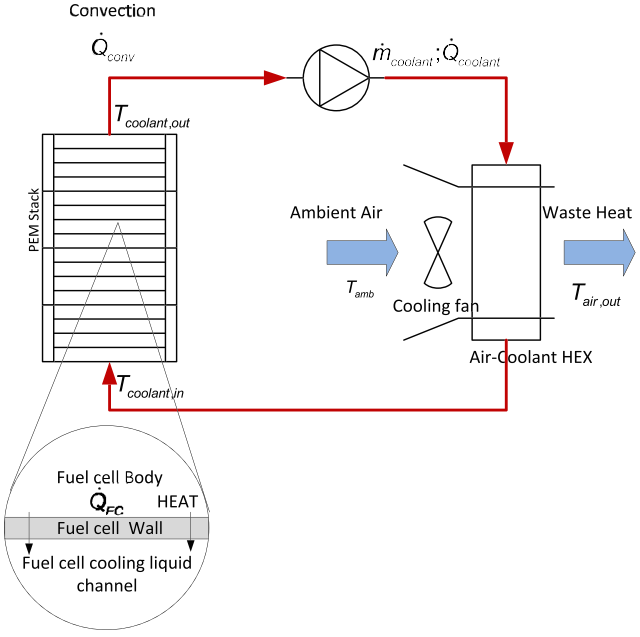

Fig. 6 – Schematic diagram of a fuel stack thermal system.

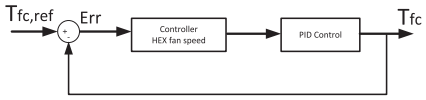

Fig. 7 – Stack temperature PID control.

The sensible heat $\dot{Q}_{sens}$ [W] represents the thermal energy variation of the gases heated in the cell estimated from the difference between the thermal energy of the gases entering into the fuel cell and the thermal energy of the unused reaction gases and other gases leaving the fuel cell. This can be neglected as its effect on stack cooling is minimal. $\dot{Q}_{coolant}$, $\dot{Q}_{air}$, $\dot{Q}_{Conv}$ are stack cooling contributions provided by the coolant, radiator-fan and convection. A_{stack} is the external surface of the stack (cm^2), K_{conv} is the convective heat transfer coefficient and $K_{conv}A_{Stack} = 10$ [$W/(m^2\ K)$], T_{FC} is the stack temperature (°C), T_{amb} (°C) is the ambient temperature, inlet air and ambient temperatures are assumed equal, $T_{air,in} = T_{amb} = 25$ °C. $\dot{Q}_{coolant}$ is dictated by fuel cell load to whereas $\dot{Q}_{air}$ is governed by the PID control as shown in Fig. 7.

The coolant heat flow rate is assumed equal to the heat dissipated by radiator-fan heat exchanger, $\dot{Q}_{coolant} = \dot{Q}_{HEX}$. The radiator air outlet temperature, $T_{Air,out}$, is calculated using the LMTD method as:

$$\dot{Q}_{HEX} = UA_{HEX}\frac{(T_{Coolant,in} - T_{Air,out}) - (T_{Coolant,out} - T_{Air,in})}{\ln((T_{Coolant,in} - T_{Air,out})/(T_{Coolant,out} - T_{Air,in}))} \quad (31)$$

The radiator UA_{HEx} value [Watt/°C] was experimentally determined as a function of the air volume flow rate $UA_{HEX} = 0.035\dot{V}_{Coolant} + 0.328$ where $\dot{V}_{Coolant}$ [l/s] is the coolant volume flow rate.

First order differential Equation (29) can be simplified as $MC_{stack} \times dT_{FC}/dt = \dot{Q}_{net}$. Evidently, this is a first-order LTI (Linear Time-Invariant) system that can be written in the form:

$$\frac{dT}{dt} + \frac{1}{\tau}T = \frac{1}{\tau} \quad (32)$$

Assuming kA_{FC} as the heat transfer coefficient for the fuel cell when heat is transferred to the coolant, the time constant, τ, assumes the following form:

$$\tau = \frac{MC_{FC}}{kA_{FC}} \quad (33)$$

The time constant says that larger stack thermal mass lead to slower changes in temperature, while larger surface areas, A_s, and better heat transfer, K, lead to faster temperature changes.

The solution to this equation suggests that, in such systems, the difference between the temperature of the stack and its coolant is given by:

Table 4 – Cathode inlet pressure and pressure drop as a function of stack current.

Fuel cell performance parameter							
Stack Current [A]	15	30	60	120	180	240	300
Cathode Nominal Inlet Pressure [kPa (abs)]	108	110	117	138	158	180	200
Oxidant Pressure Drop [kPa (abs)]	8	13	12	16	30	40	53

$$\Delta T(t) = \Delta T_0 e^{-t/\tau} \quad (34)$$

where ΔT_0 is the initial temperature difference, at time $t = 0$. The body assumes the same temperature as the coolant at an exponentially slow rate determined by the time constant. The time constant calculation is shown in Table 4. An average value of 140 kJ/K was used for MC_{FC} based on Ballard Mark V stack calculated in Ref. [1]. kA_{FC} was calculated as $kA_{FC} = \dot{Q}_{Coolant}/(\dot{V}_{Coolant}\Delta T)$ where coolant heat flow rate $\dot{Q}_{Coolant}$, volume flow rate $\dot{V}_{Coolant}$, and ΔT where experimentally determined as reported in Table 4 [2]. Coolant is a mix of water and ethylene glycol. Coolant mass flow rate was calculated assuming coolant heat capacity, $C_{P,Coolant}$, equal to 3558.78 [$J\ L^{-1}\ K^{-1}$].

In Fig. 8 step response for time constants, τ, at different stack current calculated in Table 5 is plotted. It can be seen that at higher stack current we have a faster step response to reduce temperature peaks at high loads. This is obtained increasing the coolant mass flow rate at high stack loads as shown by heat flow rate values in Table 5.

Results

In this section we show the effect of stack heat production on fuel cell system performance in dynamic conditions. The system has current as input signal. When power requested from the fuel cell stack varies, also the polarization losses change. These losses are the major contributors to stack heating.

In Fig. 9 the stack heat production is plotted when load is changed. It can be seen that temperature will increase when load is changed and smoothly decrease to the reference stack temperature is set to 65 °C. This is obtained by controlling both the liquid coolant mass flow rate and air through the radiator-fan. A fast response is required in order to avoid stack temperature changes during load changes which could fatally ruin the stack. This is ensured by controlling the coolant mass flow rate using the stack current as a reference input. A look-up table is implemented in Matlab/Simulink to relate current to coolant mass flow rate. Coolant temperature is reduced by mean of a radiator-fan which is controlled by a PID controller. For this reason air mass flow rate increases smoothly over time.

In Fig. 10 the cell IV curve and stack current vs voltage over time are plotted. In the plot a) dots represent voltage values obtained by experiment. As temperature changes, along with other factors such as cell water content, so does the magnitude of the polarization losses, even at a constant load condition. As these losses change, the output voltage of the stack is directly affected. Voltage transients are related to temperature. In particular increasing stack temperature is causing an increase in output voltage, i.e. it shifts the I–V curve upward. Therefore, in load step dynamics it can be concluded that there is a direct relationship between changing stack temperature, changing output power, and changing output voltage.

In Fig. 11, it can be seen that at low-current loads, high amounts of excess air flows is used. This is due to the fact that at low power consumption and low pressures, water is formed

Table 5 – Time constant τ calculation based experimental values of coolant temperature.

Fuel cell perfomance parameter							
Stack Current [A]	15	30	60	120	180	240	300
Coolant Inlet Temperature $T_{Coolant,in}$ [C]	60	60	60	60	60	60	60
Coolant Outlet Temperature $T_{Coolant,out}$ [C]	61	63	66	67	68	68	70
$\dot{V}_{Coolant}$ [l/s]	0.15	0.16	0.18	0.20	0.21	0.24	0.26
$\dot{Q}_{Coolant}$ [W]	521.95	1722.45	3789.39	4863.05	6113.55	6724.9	9246.74
$kA_{FC} = \dot{Q}_{Coolant}/(\dot{m}_{Coolant} \cdot \Delta T_{Coolant})$ [W/K]	521.954	574.15	631.56	694.721	764.193	840.61	924.67
τ [s]	268.22	243.83	221.67	201.52	183.2	166.54	151.40

by the reaction in the cathode side of the cells and it needs to be ejected out of the stack; this is done by supplying high amounts of air to remove the extra water. This is consistent with the cell water content shown in Fig. 2. While the amount of oxygen consumed depends on the stack current, the amount of oxygen supplied to a fuel cell is directly related to the compressor power usage. Air mass flow rate are strongly related to the stack power and were imposed using a lookup table. In real life this is done through a compressor map which univocally determines the air flow rate through the compressor RPM.

In Fig. 12 the stack gross and net power along with the system efficiency based on Hydrogen LHV at different stack current are plotted. Main contributor to the efficiency losses are stack cooling and cathode air compressor usage. A minor effect is to be accounted for the anode gas recycle pump, power conditioning and control system. Higher parasitic power losses are to be expected at higher loads. Power consumed by liquid coolant pumps is minimal and had no considerable effect on system efficiency also at high stack current. On the other hand, once the coolant thermal inertia ends is effect, the air radiator fan increases the power consumption with the result to reduce system efficiency also at constant stack current.

Conclusions

Temperature changes in PEM fuel cell are considerably higher during load variations and have a negative impact as they generate thermal stresses in the stack and reduce its lifetime. Cell hydration is also of vital importance in a fuel cell. These issues pose great important on stack thermal management and control.

This paper attempts to address the need for a control-oriented dynamic model of a PEM fuel cell system for studying temperature variations over fast load changes. For this reason, a temperature dependent cell polarization and hydration model integrated with a thermal management model was simulated in dynamic condition.

System energy balance was reduced to a first order differential equation. The first-order LTI (Linear Time-Invariant) system was used to obtain the transfer function. Time constant, τ, was determined based on experimental data at different stack loads. A feed-forward control was used to vary cathode air and hydrogen mass flow rate based on the current drawn from the fuel cell. Coolant mass flow rate was also controlled based on the current reference input. A feedback PID control was used to change the radiator-fan air mass flow rate. In order to reduce cell starvation, current ramp up and down was limited to 20 A/sec. Faster changes of the external load were assumed handled by an external electricity source (e.g. battery). Few and rapid changes in external load were imposed to study the thermal controls.

It was observed that the thermal management strategy greatly influences cell temperature and efficiency which is reduced with increase of stack load. Slow temperature controls are not recommended as they affect the stability of fuel

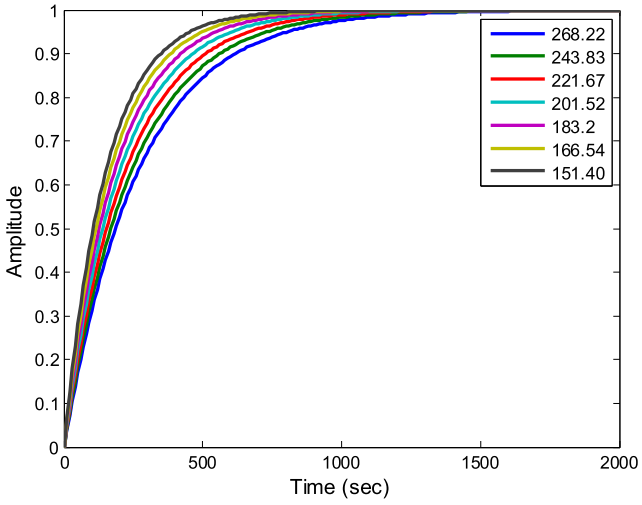

Fig. 8 – Step response of the transfer function at different time constants in Table 4.

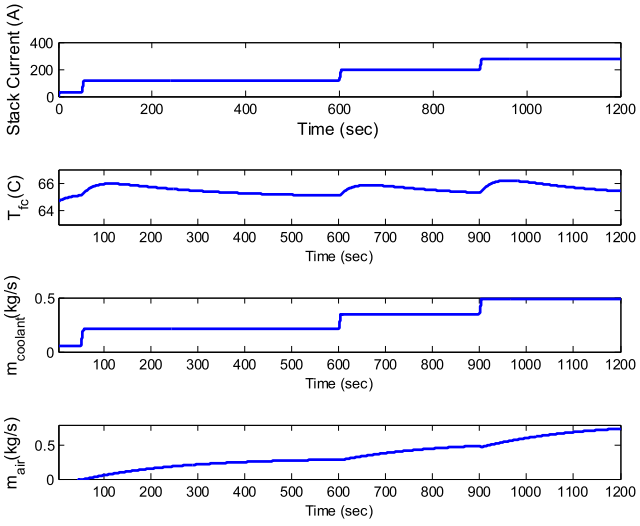

Fig. 9 – Stack heat production and temperature at different loads and the effect on coolant and radiator air fan mass flow rate.

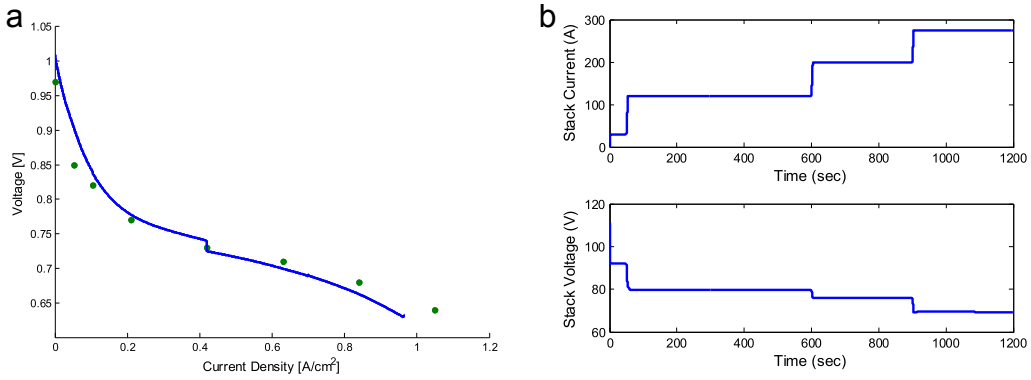

Fig. 10 – a) Cell IV curve and b) stack performance over time.

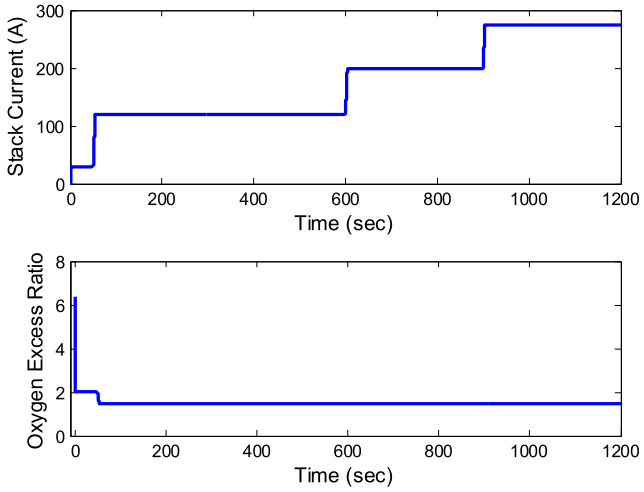

Fig. 11 – Oxygen excess at different stack currents.

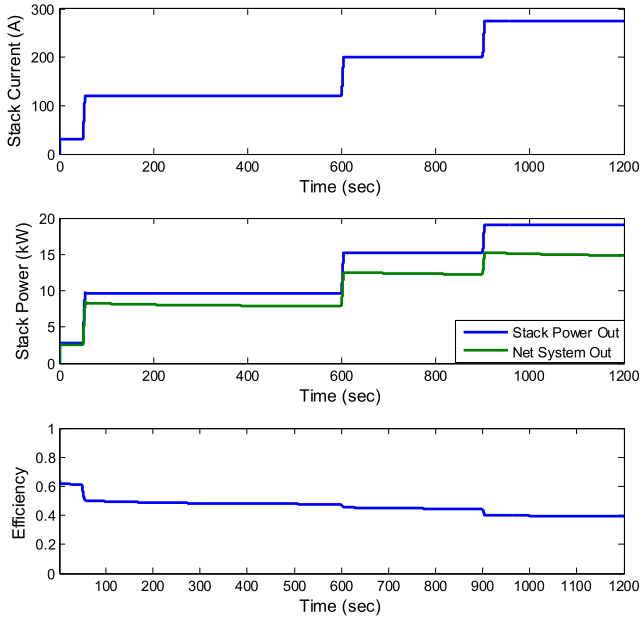

Fig. 12 – Stack gross/net power and efficiency based on hydrogen LHV at different load.

cell operations. For this reason a feed-forward control of the coolant mass flow depending on stack current input was adopted. With very high variations in coolant flow rates, power consumed by liquid coolant pumps is minimal and had no considerable effect on system efficiency. On the other hand, once the coolant thermal inertia was dissolved, the air radiator fan would increase the power consumption with the result to reduce system efficiency.

Acknowledgment

The authors would like to acknowledge the Energy Technology Development and Demonstration Program (EUDP) ID:64012E0130 for financial support and our industrial partner, H2Logic, for their collaboration and technical support.

REFERENCES

[1] Amphlett JC, et al. Performance modeling of the Ballard Mark IV solid polymer electrolyte fuel cell: I. Mechanistic model development. J Electrochem Soc 1995;142(1):1–8. Available at: http://jes.ecsdl.org/content/142/1/1.abstract.

[2] Ballard. FCvelocity®-9SSL V4 product manual and integration guide; 2011.

[3] Bao C, Ouyang M, Yi B. Modeling and control of air stream and hydrogen flow with recirculation in a PEM fuel cell system—I. Control-oriented modeling. Int J Hydrogen Energy 2006;31(13):1879–96. Available at: http://www.sciencedirect.com/science/article/pii/S0360319906001194.

[4] De Bruijn FA, Dam VAT, Janssen GJM. Review: durability and degradation issues of PEM fuel cell components. Fuel Cells 2008;8(1):3–22. http://dx.doi.org/10.1002/fuce.200700053. Available at:.

[5] Dutta S, Shimpalee S, Van Zee JW. Numerical prediction of mass-exchange between cathode and anode channels in a PEM fuel cell. Int J Heat Mass Transf 2001;44(11):2029–42. Available at: http://www.sciencedirect.com/science/article/pii/S001793100000257X.

[6] Fuller TF, Newman J. Water and thermal management in solid-polymer-electrolyte fuel cells. J Electrochem Soc 1993;140(5):1218–25. Available at: http://jes.ecsdl.org/content/140/5/1218.abstract.

[7] Hosseinzadeh E, et al. Thermal and water management of low temperature proton exchange membrane fuel cell in

fork-lift truck power system. Appl Energy 2013;104(0):434–44. Available at: http://www.sciencedirect.com/science/article/pii/S0306261912008513.

[8] Liu JG, et al. Effect of membrane thickness on the performance and efficiency of passive direct methanol fuel cells. J Power Sources 2006;153(1):61–7. Available at: http://www.sciencedirect.com/science/article/pii/S0378775305005902.

[9] Mauritz KA, Moore RB. State of understanding of Nafion. Chem Rev 2004;104(10):4535–86. Available at: http://www.ncbi.nlm.nih.gov/pubmed/15669162.

[10] Motupally S, Becker AJ, Weidner JW. Diffusion of water in Nafion 115 membranes. J Electrochem Soc 2000;147(9):3171. Available at: http://jes.ecsdl.org/cgi/doi/10.1149/1.1393879.

[11] Pukrushpan J. Modeling and control for PEM fuel cell stack system. Am Control:3117–22. Available at: http://ieeexplore.ieee.org/xpls/abs_all.jsp?arnumber=1025268; 2002 [accessed 05.07.13].

[12] Rabbani RA, Rokni M. Dynamic simulation of a proton exchange membrane fuel cell system for automotive applications; 2012 (June). pp. 311–6.

[13] Vasu G, Tangirala AK. Control-orientated thermal model for proton-exchange membrane fuel cell systems, 183; 2008. pp. 98–108.

[14] Yu X, Zhou B, Sobiesiak A. Water and thermal management for Ballard PEM fuel cell stack. J Power Sources 2005;147(1–2):184–95. Available at: http://www.sciencedirect.com/science/article/pii/S0378775305001618.

[15] Zawodzinski TA, et al. Water uptake by and transport through Nafion® 117 membranes. J Electrochem Soc 1993;140(4):1041–7. Available at: http://jes.ecsdl.org/content/140/4/1041.abstract.